Pergamon

Chaos, Solitons & Fractals Vol. 5, Nos 3/4, pp. 513–526, 1995

0960-0779/95$9.50 + .00

0960–0779(93)0039–E

Dynamics of Rotating Vortices in the Beeler–Reuter Model of Cardiac Tissue

IGOR R. EFIMOV,*† VALENTIN I. KRINSKY*‡ and JOSE JALIFE§

*Institute of Theoretical and Experimental Biophysics, Russian Academy of Sciences, 142292 Pushchino, Moscow Region, Russia, †Department of Physiology, University of Pittsburgh, School of Medicine, Pittsburgh, PA 15261, USA, ‡Institute Non Lineaire de Nice UMR C.N.R.S. 129, Universite de Nice, Sophia Antipolis, Parc Valrose, F 06034 Nice Cedex, France, §Department of Pharmacology, SUNY Health Science Center at Syracuse, 766 Irving Avenue, Syracuse, NY 13210, USA

Abstract—Cardiac muscle is a highly nonlinear active medium which may undergo rotating vortices of electrical activity. We have studied vortex dynamics using a detailed mathematical model of cardiac muscle based on the Beeler–Reuter equations. Specifically, we have investigated the dependence of vortex dynamics on parameters of the excitable cardiac cell membrane in a homogeneous isotropic medium. The results demonstrate that there is a transition from the vortex with circular core that is typical of most excitable media, including the Belousov–Zhabotinsky reaction, to a vortex with linear core that has been observed in heart muscle during so-called reentrant arrhythmias. The transition is not direct but goes through the well-known sequence of nonstationary quasiperiodic rotating vortices. In the parameter space there are domains of different types of vortex dynamics. Such domains include regions where: (1) vortices can not be generated, (2) vortices occur readily, and (3) vortices arise but have a short lifetime. The results provide testable predictions about dynamics associated with initiation, maintenance and termination of cardiac arrhythmias.

1. INTRODUCTION

Cardiac muscle contracts periodically about once per second. Every contraction is initiated by an electrochemical wave that spreads at about 0.5 $m\,s^{-1}$. When the wave reaches a cell, its membrane potential jumps by 100 mV over approximately 2–3 ms and slowly returns to the resting state over several hundred ms (see Fig. 1). The cardiac wave is a strongly nonlinear wave whose amplitude and shape do not change during propagation. In this respect, it resembles a soliton, although the mechanisms of its propagation are quite different from those of the soliton which spreads without decay only in one-dimensional media. In contrast, the electrochemical wave in the heart does not decay even in two or three dimensions. Moreover, as any other wave, the electrochemical wave in the heart can diffract according to Huyghens' principle. However, its behavior is somewhat similar to that of particles in that two colliding waves annihilate each other. In this respect also, the cardiac wave is extremely different from colliding solitons, which can penetrate one another.

The simplest equation describing a wave with the foregoing properties can be written in the form of a reaction–diffusion equation:

$$dU/dt = D\triangle U + f(U),$$

where $D\triangle U$ is the diffusion term and $f(U)$ is a nonlinear function (often of a special type, used by van der Pol [26] for description of electrical impulse generator). For scalar U, this

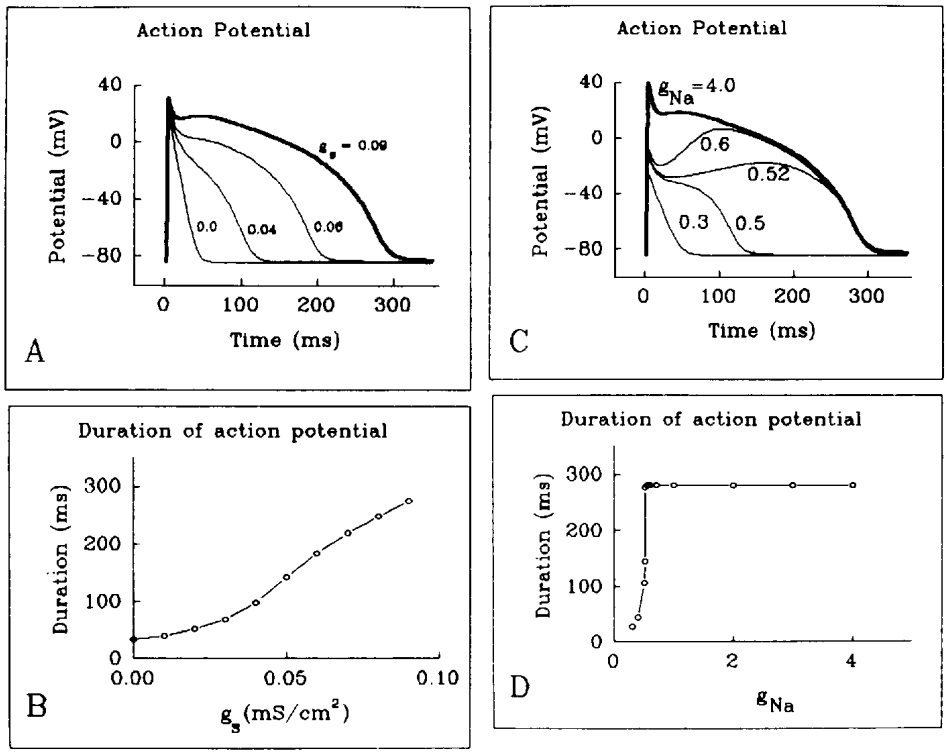

Fig. 1. Action potential of the cardiac muscle. Bold line corresponds to normal cardiac tissue. Thin lines correspond to various levels of suppression of conductance g_s (in mS cm^{-2}) for slow (Ca) current. Calculation of BR equations using normal values of other parameters.

equation is called the KPPF equation [15, 35]. On the other hand, when **U** is a two-component vector and function f is a cubic, the above equation is called the FitzHugh–Nagumo (FHN) equation. However, natural excitable media should be described by more complex equations. For example, in the case of the Hodgkin and Huxley model [12] of nerve fiber, vector **U** contains 4 components; in the Beeler and Reuter model [4] of the heart muscle, vector **U** consists of 8 components describing various ionic currents and membrane voltage. In two-dimensional space, all these equations have interesting solutions in the form of rotating vortices (spiral waves). Such vortices underlie various phenomena in natural excitable media; for instance, they are involved in the control of morphogenesis in colonies of the social amoebae *Dictyostelium discoideum*, promoting species' survival [10]. In the heart, rotating vortices are a major cause of life-threatening rhythm disturbances such as tachycardia and fibrillation.

Rotating spiral waves were predicted to be a mechanism of a cardiac arrhythmias by Wiener and Rosenblueth [27]. Later, the hypothesis was brilliantly confirmed by the experiments of Allessie *et al.* [2] in cardiac tissue. Moreover, over the years, spiral waves have been shown to be a basic feature of excitable media of diverse nature; for example, vortex waves of electrochemical activity may develop when an iron grid is immersed in nitric acid [25]; rotating waves of concentration may develop also in the chemical reaction known as the Belousov–Zhabotinsky (BZ) reaction [5, 30, 31]; spiral waves of spreading depression have been demonstrated in the retina of birds [11]; and spiral calcium waves have been found in the cytosol of *Xenopus oocytes* [17].

Vortices in heart muscle differ from well-studied vortices in the BZ chemical reaction and from those obtained in numerical simulations of cardiac tissue in that they display

essentially distinct dynamics. Indeed, in the majority of computational and chemical experiments, the tip of a spiral wave rotates around a stationary or moving center (core) that is almost circular in shape (Fig. 2(A)). In contrast, in myocardium, the tip of the vortex traces a trajectory that consists of a straight-line segment and sharp turns (Fig. 2(C)).

What causes such a qualitative difference? In cardiology, it is common to consider the anisotropy of myocardium to be the main mechanism because myocardium consists of elongated cells oriented end to end, and the velocity of wave propagation along cells is about 3 times greater than across cells [24]. Whether the shape of the vortex core in the heart is a consequence of its anatomical specificity or a generic property of highly nonlinear autowave media is still in question. Vortices with stable linearly shaped cores similar to those observed in cardiac muscle were found in the FitzHugh–Nagumo equation [16]. We have now extended our observations of core dynamics using a mathematical model of isotropic and homogeneous cardiac muscle. The main purpose of the present study was to use the BR equations [4] to investigate: (i) shapes of vortex cores; (ii) bifurcations from circular to linear vortex cores; and (iii) parameters that can affect formation, dynamics, and termination of rotating vortices.

2. MODEL AND PROCEDURE USED IN NUMERICAL EXPERIMENTS

Numerical experiments were performed using the BR model which consists of 8 differential equations (1–3). Equation (1) describes the membrane potential V:

$$\frac{dV}{dt} = D\triangle V - \frac{1}{C}(i_{k1} + i_{x1} + i_{Na} + i_{Ca} - i_{ext}), \tag{1}$$

where C = membrane capacitance, V = membrane potential, i_{k1} = time-independent potassium outward current, i_{x1} = time-activated outward current, i_{Na} = initial fast inward current carried primarily by sodium ions, i_s = secondary or slow inward current carried mainly by calcium ions.

The time derivative of calcium ion concentration, [Ca], is given by the equation:

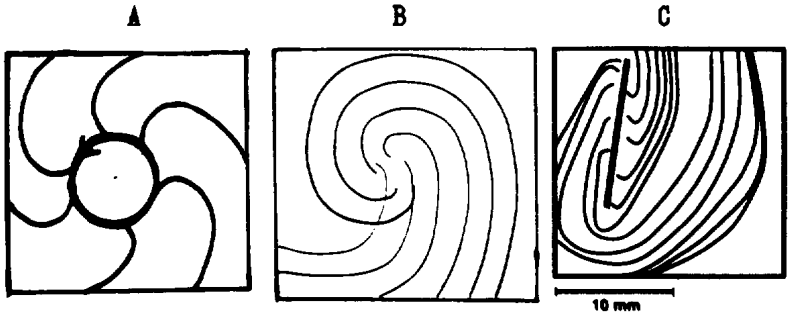

Fig. 2. Rotating vortex in cardiac muscle and mathematical models. (A) Vortex in numerical experiments using the simplest (FitzHugh–Nagumo) model of excitable media. Thin lines represent consecutive positions of the activation front. Bold circle in the center is the core of the vortex (a trajectory of the front break). An arrow indicates the direction of rotation. (Adapted from Zykov [33] by permission). (B) Vortex in numerical experiments on a modified BR model of ventricular myocardium. Wavefronts are depicted at intervals of 0.04 s (from Winfree [30] by permission). (C) Activation map of spiral wave activity in a thin slice of isolated ventricular cardiac muscle (from Davidenko *et al.* [8], by permission). The fronts were recorded every 16.6 ms. The mapping was carried out using a potentiometric dye probe and video imaging with a spatial resolution of 500 μm after filtering. The bold line indicates the vortex core in this case. Clearly, the core in the heart muscle differs qualitatively from that in the mathematical models shown in (A) and (B): the point of wavefront break moves along a line in cardiac tissue, and along a circle in both mathematical models.

$$\frac{d[Ca]}{dt} = -10^{-7} i_s + 0.07(10^{-7} - [Ca]). \tag{2}$$

The dependence of the membrane current on time, the membrane potential and the parameters of activation and inactivation are described in the Appendix. The time derivatives of these parameters, x_1, m, n, j, d, and f, are given by the equation:

$$\frac{dY_i}{dt} = \frac{(Y_i - \bar{Y}_i)}{\tau_i}, \tag{3}$$

$\bar{Y}_i$ and τ_i are defined in the Appendix (Y_i is replaced by the corresponding activation or inactivation parameter).

The following modifications were made in an effort to speed up the calculations and reduce the computational cost of using the BR:

(1) The sodium activation parameter (i.e. variable m in equation (3)) was reduced to the steady state; it was then stored as a function of V (from -100 mV to 50 mV) with steps of 1 mV, and linearly interpolated during calculations.

(2) Since the original model includes a large number of exponents and a logarithm (see Appendix, equations (A.1, A.4, A.5 and A.3)) that take much time for calculation, we used a standard procedure that allows their tabulation as functions of V; we used the same voltage range and voltage step as for variable m, and linearly interpolated the data in the process of calculation. The error thus introduced was less than 1%.

Experiments were performed using a matrix of 100×100 elements. Integration was carried out using the Euler method in cartesian coordinates; Neumann boundary conditions ($\partial E/\partial n = 0$) were used. In some simulations, a 300×300 grid was used with standard parameters in order to test the accuracy of the calculations of the linear core vortex. The space step $\Delta x = 0.25$ mm and the time step $\Delta t = 0.1$ ms. Errors in the velocity, amplitude and duration of the action potential were determined by comparing the membrane potential response of a modified unidimensional model to stimulation with the simultaneously induced response of the unmodified (i.e. without reduction of the variable m) unidimensional model. Calculations in the latter were carried out at $\Delta x = 0.01$ mm and $\Delta t = 0.005$ ms. An error of 12% resulted from the different Δx and Δt, as well as from the reduction of the variable m to its steady-state value.

The initial conditions were similar to those used commonly to obtain a plane excitation wave with broken wavefront [33]. The spatial distribution of i_{Na} was used to determine the position of the wavefront and vortex tip by constructing a binary array from the array of i with a threshold of 0.05 $\mu A\,cm^{-2}$. The picture thus obtained corresponded to a long line whose thickness was 2–4 pixels. The line was parametrically described and its tip was found.

3. RESULTS OF NUMERICAL EXPERIMENTS

3.1. *Two kinds of vortices in the BR model*

Cardiac muscle undergoes highly relaxational pulses of electrical activity; the characteristic risetime of the wavefront is about 2–3 ms and that of the plateau is roughly 100 times larger (see Fig. 1, bold line). Numerical simulation of such highly relaxational media is time-consuming even when using a supercomputer, and requires special computational methods. Thus, in their calculations, researchers usually have to use parameter values that make the equations less complicated. These parameter values cause the so-called 'good' vortices (i.e. with almost circular cores, see Fig. 2(A)) that are usually observed in the BZ reaction, as well as in populations of social amoeba *Dyctiostelium discoideum*. An example

of the vortex calculated using the modified BR model is shown in Fig. 3. The appearance of the vortex varies depending on which variable is displayed: membrane potential in panel A, calcium concentration in panel B and sodium current in panel C. Note, for example, that the sodium current is restricted to a narrow band at the very front of the excitation wave. Yet, regardless of the display, the vortex is always a 'good' one, because its circular core is typical of that of many excitable nonlinear media that are not too stiff. But such vortices are not typical for cardiac muscle, in which the core is not circular at all (see Fig. 2(C)).

Linear-type vortex cores may be demonstrated in the BR model when parameters corresponding to the normal myocardium [4] are used. In Fig. 4 we show a linear core obtained during 5 rotations of the vortex with steps $\Delta x = 0.5$ mm and $\Delta t = 0.5$ ms; the core shape was re-checked for two rotations with steps $\Delta x = 0.25$ mm and $\Delta t = 0.1$ ms. Suppression of ionic conductances g_{Na} and g_s resulted in decreased stiffness (see Fig. 1), and in a transition from linear to circular core, but the type of vortex obtained did not depend on the initial conditions (for further details see Krinsky *et al.* [16]).

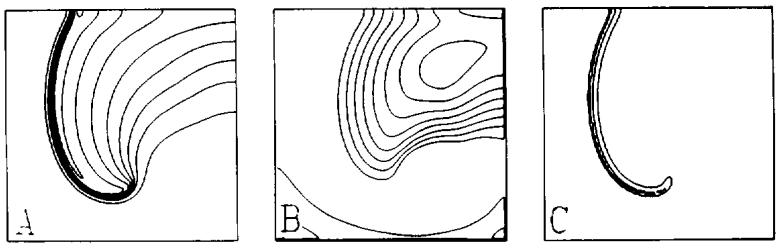

Fig. 3. A vortex in the BR model of myocardium. (A) membrane potential distribution, isolevels from −80.0 to 0.0 mV with 10 mV step. (B) intercellular calcium concentration distribution, isolevels from 0.1×10^{-7} to 20.0×10^{-7} l mole^{-1} with 0.2×10^{-7} l mole^{-1} step. (C) fast inward (sodium) current distribution, isolevels 0.05 and 0.6 μA cm^{-2}. Calculation on a mesh of 100×100 elements, steps $\Delta x = 0.25$ mm, $\Delta t = 0.1$ ms. Parameter $g_{Na} = 2.2$ mS cm^{-2}, $g_s = 0.045$ mS cm^{-2} (half of normal value of maximum conductances).

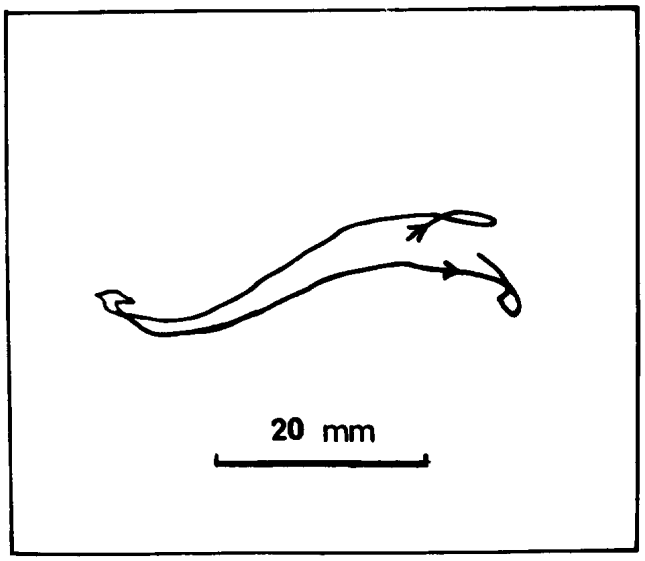

Fig. 4. Vortex tip trajectory in the BR model ($g_{Na} = 4.0$ mS cm^{-2}, $g_s = 0.09$ mS cm^{-2}). Simulation using a mesh of 200×200 elements with steps $\Delta x = 0.5$ mm, $\Delta t = 0.5$ ms. Here the trajectory is qualitatively similar to that of the cardiac muscle (Fig. 2(C)).

3.2. *Types of vortex circulation in the BR model*

As illustrated in Fig. 5, variation of parameters led to a transition from circular to linear cores. Indeed, when g_{Na} is changed from 2.1 to 2.2, the stiffness of the equation is slightly increased. Under these conditions, the circular rotations become unstable, and the trajectory of the tip begins to resemble an epicycloid. It then becomes similar to a cycloid ($g_{Na} = 2.3$), and a hypocycloid ($g_{Na} = 2.5$). Finally, when g_{Na} is increased to 4.0, the trajectory becomes linear such as that observed in cardiac muscle (see Fig. 2(C)).

The type of symmetry-breaking shown in Fig. 5 is well known to occur in simpler models of excitable media. The transition from periodic circular motion to quasiperiodic two-frequency motion is shown to be a Hopf bifurcation [3]. Cycloidal-like circulation was described by Zykov [32] and by Lugosi [18] for the FitzHugh–Nagumo model; by Fast *et al.* [9] for a cellular automata model; by Jahnke *et al.* [13], and Jahnke and Winfree [14] for the Oregonator model, as well as by Agladze [1] and by Skinner and Swinney [23] for the BZ reaction.

The parameter space $g_s - g_{Na}$ contains areas with various types of spiral wave circulation (and tip trajectories), as illustrated in Fig. 6. Four types are shown: circular (area A), epicycloidal (area B), cycloidal (line C), and hypocycloidal (area D). Since calculations in the parameter range corresponding to the linear vortex cores consume much computer time, they were performed only for several points ($g_{Na} = 3.5$, 4.0, 5.0, 6.0, mS cm^{-2} and standard $g_s = 0.09$ mS cm^{-2}); thus, the area in parameter space corresponding to the linear cores was not determined.

3.3. *Qualitative analysis of the vortex circulation pattern*

A kinematic theory describing the dependence of the circulation radius on the parameters of the medium was proposed by Zykov *et al.* A model of cycloidal circulation was developed in ref. [33] and in ref. [18]. However physical mechanisms have not yet been proposed for the transitions from circular to epicycloidal, then to cycloidal, hypocycloidal, and linear-type trajectories.

Let us consider qualitatively the mechanism of these changes. For discussion purposes, we shall use the term curvature to describe the trajectory of the vortex tip motion rather

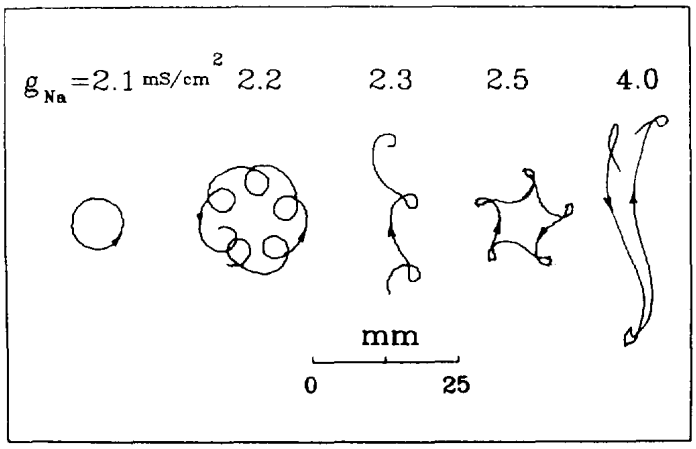

Fig. 5. Transition from circular to quasilinear vortex core. Maximum sodium conductance g_{Na} is indicated on top. Parameter $g_s = 0.09$ mS cm^{-2} was used for the rightmost picture, and $g_s = 0.045$ mS cm^{-2} was used elsewhere. Simulation using a mesh of 150 × 150 elements.

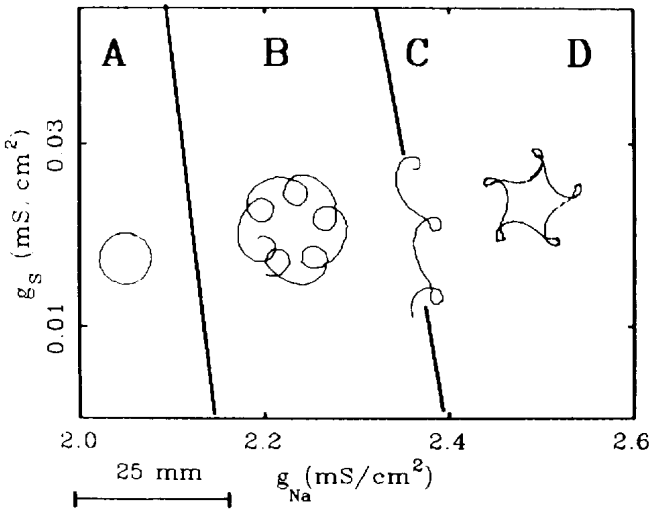

Fig. 6. Types of tip trajectories in parameter space (g_{Na} and g_s). (A) region of circular shape. (B) region of epicycloidal shape. (C) border line of cycloidal shape. (D) region of hypocycloidal shape. Simulation was done using a mesh of 150 × 150 elements with steps $\Delta x \times 0.25$ mm, $\Delta t = 0.1$ ms. All the depicted trajectories were calculated with fixed $g_s = 0.045$ mS cm^{-2} and varied g_{Na}.

than to indicate the shape of the wavefront. In area (A) of Fig. 6, the curvature of the trajectory associated with circular movement is positive and fixed. In area (B), the trajectory of the vortex tip consists of small loops and large arcs. When parameter g_{Na} is increased, the relative position of the loops and arcs varies and the trajectory becomes straight (line (C)); subsequently, as g_{Na} is further increased, the trajectory closes (area (D)) but the direction of the loops and arcs is opposite to that in (B). The curvature of the trajectory of the epicycloid (Fig. 6(B)) is everywhere positive; in the hypocycloid (Fig. 6(D)), however, the negative curvature predominates. The cycloid (Fig. 6(C)) is intermediate in that curvature is positve almost everywhere except at the inflection point, where it is zero. The curvature along the trajectories is displayed in Fig. 7 for all such cases. It may be observed that the curvature changes periodically for all cycloidal-type trajectories. Thus, the question of origin of cycloidal-type trajectories can be reduced to the origin of periodical changes in the curvature. We will show that: (1) for all types of cycloids there is a periodic motion whereby each wave first approaches and then lags behind the preceding wave, which results in periodic modulation of the excitability and, as a consequence, the curvature; (2) for circular trajectories each wave moves at a constant distance from the preceding wave, which maintains both excitability and curvature fixed.

It is well known that decreasing the excitability (i.e. increasing the excitation threshold) results in a decrease in the wavefront critical curvature, as well as in transitions from positive to negative critical curvature values. However, the analogy is misleading since it concerns the curvature of the wavefront rather than the trajectory of the wavebreak trajectory. To understand the transitions between trajectory types it is useful to think in terms of wavebreak evolution. Figure 8 shows three different types. In panel (B), the propagating broken wavefront does not change its length (the break point moves normally to the front). In panel (C), the wavefront propagates in a medium with decreased excitability (increased excitation threshold) and, as a result, the broken wavefront shortens during propagation. In Fig. 8(A) the wavefront propagates in a medium with increased excitability (decreased excitation threshold) and lengthens. It is clear that the curvature is zero in panel (B) (the wavebreak moves along a straight line), positive in panel (A) and

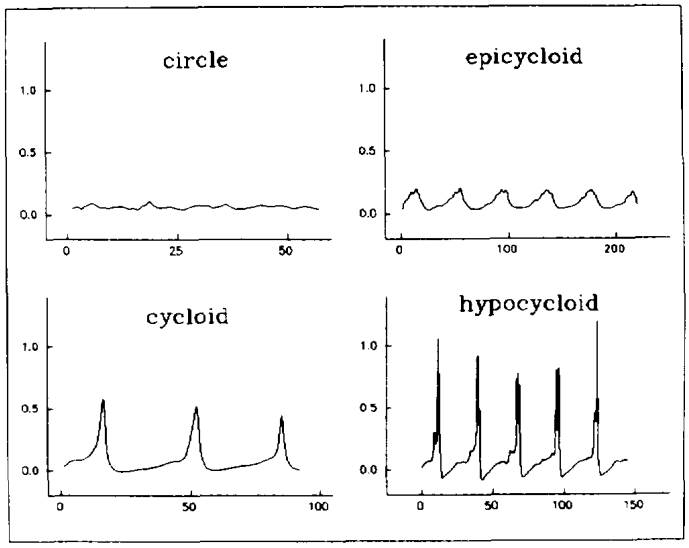

Fig. 7. Vortex wavebreak trajectory curvature vs its length. Circle $g_{Na} = 2.1\ mS\,cm^{-2}$; epicycloid $g_{Na} = 2.2\ mS\,cm^{-2}$; cycloid $g_{Na} = 2.3\ mS\,cm^{-2}$; hypocycloid $g_{Na} = 2.5\ mS\,cm^{-2}$. A mesh of 150 × 150 elements was used for the simulation. For all the trajectories, $g_s = 0.045\ mS\,cm^{-2}$.

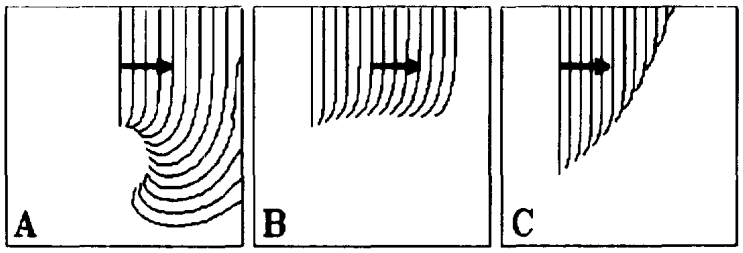

Fig. 8. Various regimes of wavebreak propagation in BR model: (A) wavefront lengthens ($g_{Na} = 2.1\ mS\,cm^{-2}$). (B) wavefront does not change its length ($g_{Na} = 2.0\ mS\,cm^{-2}$). (C) wavefront shortens ($g_{Na} = 1.9\ mS\,cm^{-2}$). A mesh of 100 × 100 elements was used with steps $\Delta x = 0.25$ mm, $\Delta t = 0.1$ ms. Parameter $g_s = 0.03\ mS\,cm^{-2}$.

negative in panel (C). Thus the mechanism of the cycloidal types of trajectories of Fig. 5 can be explained quite simply as follows: the periodic approaching and lagging of the wavefront in relation to the preceding wave causes a periodic modulation of the excitability and the curvature, which gives rise to the cycloids. Which type of cycloidal curve (epicycloid, hypocycloid or cycloid) will be observed depends on how close each wavefront comes to the preceding wave and thus on how deeply the excitability is depressed.

Numerical proof for the above statement is presented in Fig. 9. In the top panel, the variations in threshold associated with changes in the position of the wavebreak along a hypocycloid are depicted as changes in the thickness of the curve. The threshold values were estimated according to the data plotted in the lower panel, which shows the time course of threshold and calcium concentration during a single action potential in a BR cell. Clearly, threshold increases when the wavebreak traces a big arc of the hypocycloid because it propagates close to the preceding wave; threshold decreases when the wavebreak outlines a highly curved loop of a hypocycloid because it propagates far from the preceding wave.

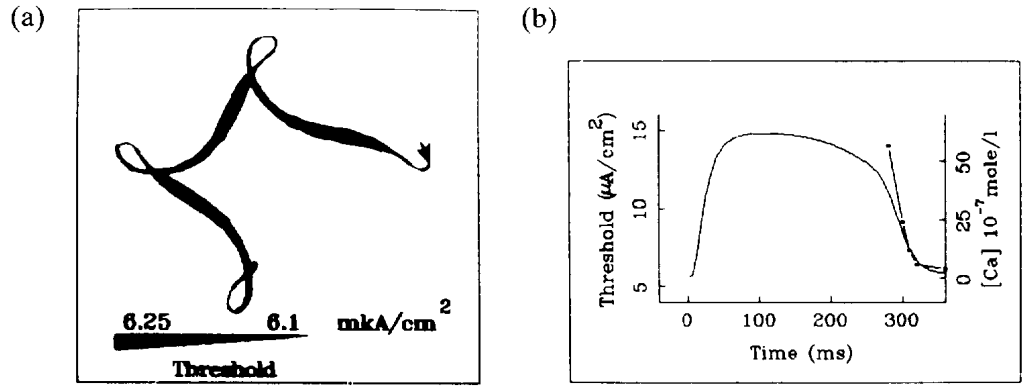

Fig. 9. (a) Threshold of excitation along hypocycloidal vortex tip trajectory. The threshold was estimated from the calcium concentration (using panel (B) for construction of calibration curve). Calculation on a mesh of 150 × 150 elements. Parameters $g_s = 0.045\ \mathrm{mS\,cm^{-2}}$, $g_{Na} = 2.5\ \mathrm{mS\,cm^{-2}}$. (b) Threshold of excitation (dotted) and calcium concentration (solid) during action potential.

3.4. *Detailed description of the trajectory*

As shown in Fig. 10, three characteristics can be used to describe a cycloid: the radius r_k of the loop, the distance l_k between neighboring loops and the angle φ formed by three successive loops. Angle φ is greater than 180° for the epicycloid; it is equal to 180° for the cycloid; and less than 180° for the hypocycloid. Moreover, from calculations similar to those shown in Figs 5 and 11, one can see that r_k decreases if g_{Na} is increased (Fig. 5); r_k does not depend on g_s (Fig. 11); the distance between loops l_k increases if g_{Na} or g_s are increased (Fig. 11); angle φ decreases if g_{Na} is increased (see Fig. 5), and φ does not depend on g_s (Fig. 11). Let us now describe the physical mechanisms underlying these dependencies. It is convenient to do this by using physical notions of relaxation time and threshold of excitation. In electrophysiology the term refractoriness is used instead of relaxation time, and the term excitability is used as the inverse of threshold of excitation (an increase of threshold is equivalent to a decrease of excitability). It is well known that relaxation time is governed by calcium channel conductance g_s (i.e. an increase in g_s leads to an increase in relaxation time) and depends little on g_{Na}. On the other hand, threshold of excitation is governed by sodium channel conductance g_{Na} (i.e. a decrease in g_{Na} leads to a decrease in excitability), but does not depend on g_{Na}.

The radius r_k of the loop decreases when g_{Na} is increased because, when the excitability increases, the curvature of the wavebreak trajectory also increases (see Section 3.3). The

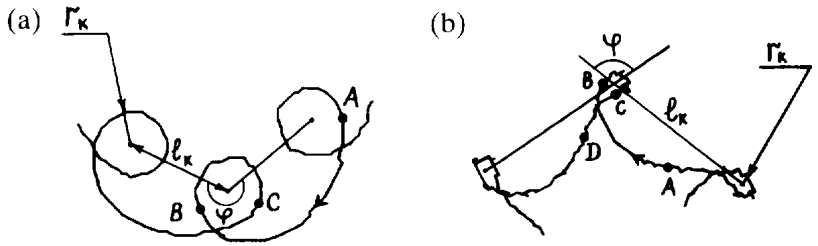

Fig. 10. Geometrical characteristics of vortex tip trajectories with a hypocycloid (a) and an epicycloid (b) as examples: r_k = radius of turn in the unexcited medium (loop radius), l_k = distance between loops, φ = angle between loops, AB = an ark with large radius, BC = an ark with small radius, CD = an ark with negative curvature.

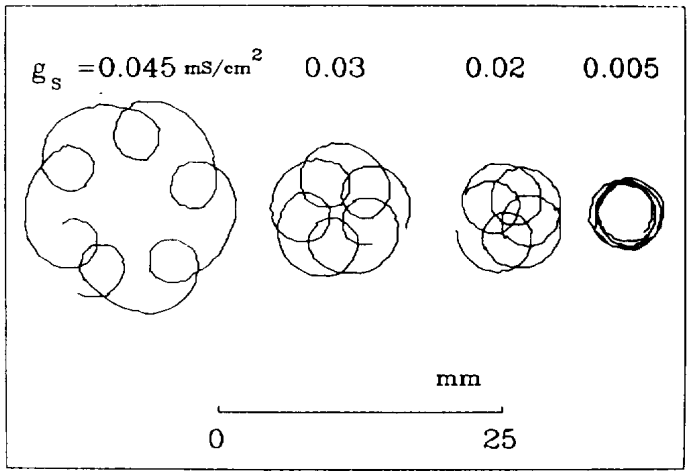

Fig. 11. The transition from circular to cycloidal circulation induced by increase in maximum calcium conductance g_s. Parameter g_{Na} is fixed (2.2 mS cm^{-2}).

distance between loops l_k increases if either g_{Na} or g_s is increased (Fig. 11). There are two reasons for this: firstly, an increase of g_s leads to an increase in refractoriness and, consequently, to an increase in the length of the segment of trajectory that is situated within the refractory region; secondly, when g_{Na} increases r_k decreases; as a result after undergoing a loop, the wavebreak appears early within the refractory phase, which further increases the length of the segment of trajectory that is located within that phase.

4. DISCUSSION

The Beeler and Reuter equations simulate cardiac electrical activity in a similar manner to that in which the equations used by Hodgkin and Huxley simulate the action potential of the squid giant axon. The approach is based on measurements of local properties by means of voltage and space-clamp experiments, and the description of the distributed system is made on the basis of physical principles by the addition of the diffusion term. Of course, it was necessary to carry out experiments to check the validity of the partial differential equations. In the case of the Hodgkin and Huxley equations, one-dimensional experiments with measurements of pulse-propagation velocity were sufficient. On the other hand, predictions derived from any extended model of cardiac muscle require biological experiments in two or three dimensions. To our knowledge, comparison between results of simulations using the BR equations and those of experiments in two-dimensional cardiac muscle has not been made to date. This is the first demonstration that, under the appropriate circumstances, the BR equations may result in vortices with stable linear cores, which are typical of those in cardiac muscle.

Vortices with linear cores were found initially in the classical formulation of Wiener and Rosenblueth [27, 36, 37, 38]. Later, experimental findings in an active chemical medium (summarized in ref. [31] see also [27, 36, 37, 38]) confirmed all major results obtained earlier with the automata model of Wiener and Rosenblueth, with one important exception: the form of the vortex core; in the chemical medium the wave rigidly rotated around a circle instead of moving around a line. Subsequent numerical simulations using partial differential equations [40] yielded similar results. Since then, all calculations that have been published (see review by Winfree [39]) have confirmed the previous results and

many new beautiful examples of rotating vortices have been presented (see, for example, refs [17, 21]). In most cases, however, the core of the vortex is circular in shape. Recent refinements have led to the discovery of unstationary wave rotations in simulations [32, 3] and experiments using active chemical media [28, 13]. During such unstationary circulation, elongated trajectories have been observed in both computer simulations [7] and in experiments using the chemical active medium [19]. Yet, vortices resembling those described originally by Wiener and Rosenblueth's model have been found in cardiac muscle only. It is important to remember, however, that cardiac muscle is a highly anisotropic, discrete excitable medium which, as a result of spatial scaling, may give rise to vortices with elongated cores. In addition, experimental approaches used in the past to record rotating vortices in cardiac muscle by means of multiple-electrode mapping systems did not have the appropriate space resolution to enable the visualization of vortex cores. The recent introduction of optical mapping and video imaging technology to the study of vortex-like activity [8] has provided a direct means of directly addressing these issues [16]. Thus, it is now clear that:

(i) Linear cores are not an artifact of the automata model but real phenomena which may appear in continuous homogeneous media. Whether or not a linear core will be observed, will depend on the ratio of the two characteristic scales—the wavelength λ and the minimal radius r of the wavefront curvature. If $r > \lambda$, the usual circular core is observed, for $r \ll \lambda$, a linear core will arise.

(ii) Elongated trajectories observed during unstable circulation are in fact transitions from circular to elongated cores.

(iii) To observe the transition from elongated to less elongated core in cardiac muscle, it would be necessary to increase the dimensionless value r/λ which, as shown in the present paper, may be achieved by decreasing the Na^+ and Ca^{2+} conductances.

The simulation of excitation waves in the Beeler and Reuter model with reduced sodium current, mimics the effects of certain antiarrhythmic drugs, and the results presented here provide a plausible mechanism for some of the beneficial actions of such drugs.

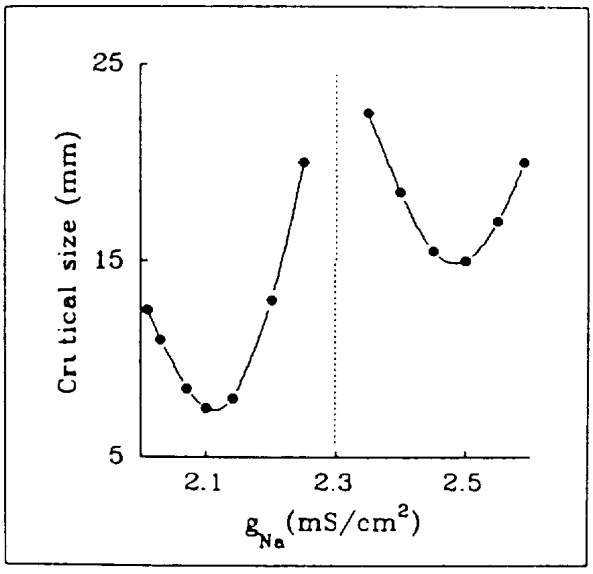

Fig. 12. Minimum size of the medium in which vortex can subsist indefinitely as a function of maximum sodium conductance (g_{Na}) at fixed $g_s = 0.045\ mS\,cm^{-2}$. When $g_{Na} = 2.3\ mS\,cm^{-2}$, the critical size goes to infinity (the trajectory becomes cycloidal).

By reducing the excitability, the drug may convert a linear core of a vortex into a cycloid (Fig. 5). Under these conditions, the vortex tip would move close to a boundary of the medium (e.g. an artery or a scar) and the rotating activity would vanish. The results may help also to explain the concept of minimal (critical) size of heart muscle in which vortex-like activity can be sustained. As shown in Fig. 12, at $g_{Na} = 2.3\ mS\,cm^{-2}$ the critical size becomes infinite; i.e. the vortex cannot exist a sufficiently long time in a bounded medium. This result suggests that an appropriate dose of an antiarrhythmic drug may benefit the patient, whereas a slightly different dose may not. For instance, when the conductance changes from the normal value of $g_{Na} = 4.0\ mS\,cm^{-2}$ to $g_{Na} = 2.5\ mS\,cm^{-2}$, the effect will be weak and the arrhythmia would not disappear. The critical size grows remarkably only at $g_{Na} = 2.310\ mS\,cm^{-2}$. Under these conditions, the vortex-like activity would be terminated and the antiarrhythmic therapy would be a success. Overdosing ($g_{Na} < 2.2\ mS\,cm^{-2}$) would reduce the critical size and the antiarrhythmic effect would again disappear.

The present work shows that, despite its remarkable complexity (8 equations), the Beeler and Reuter model is not a monster among differential equations describing simple excitable media. It describes the generic features of vortex dynamical behavior in the heart muscle.

Acknowledgments—We are grateful to Drs A. M. Pertsov and E. A. Ermakova for help in the BR model; Professor S. E. Shnoll and A. T. Winfree and Drs V. G. Fast, V. N. Biktashev and A. V. Panfilov for many helpful discussions. This work was supported in part by grants HL-39707 and HL-29439 (to J. J.) from the National Heart Lung and Blood Institute.

REFERENCES

1. K. I. Agladze, Studying of rotating spiral waves in chemical excitable media, preprint. NCBI, Pushchino, USSR (1983). (in Russian)
2. M. A. Allessie, F. I. M. Bonke and F. J. C. Schopman, Circus movement in rabbit atrial muscle as a mechanism of tachycardia, *Circ. Res.* **33**, 54–62 (1973).
3. D. Barkley, M. Kness and L. S. Tuckerman, Spiral wave dynamics in a simple model of excitable media: The transition from simple to compound rotation, *Phys. Rev.* **42**, 2489–2492 (1990).
4. G. W. Beeler and H. Reuter, Reconstruction of the action potential of ventricular myocardium fibers, *J. Physiol.* **268**, 177–210 (1977).
5. B. P. Belousov, Oscillating reaction and its mechanism, in *Sbornik referatov po radiacionnoi medicine*, p. 145 (1959). (in Russian)
6. F. J. L. van Capelle and D. Durrer, Computer simulation of arrhythmias in a network of coupled excitable elements, *Circ. Res.* **47**, 454–466 (1980).
7. M. Courtemanche and A. T. Winfree, Re-entrant rotating waves in a Beeler–Reuter based model of two-dimensional cardiac electrical activity, *Int. J. Bifurcation & Chaos* **1**, 431–443 (1991).
8. J. M. Davidenko, A. M. Pertsov, R. Solomonsz and J. Jalife, Stationary and drifting waves of excitation in isolated cardiac muscle, *Nature, Lond.* **355**, 349–351 (1992).
9. V. G. Fast, I. R. Efimov and V. I. Krinsky, Transition from circular to linear rotation of a vortex in an excitable cellular medium, *Phys. Lett.* **A151**, 157–161 (1990).
10. G. Gerisch, Cell aggregation and differentiation in *Dictyostelium*, in *Current Topics in Development Biology*, edited by A. Moscona and A. Monroy, Vol. 3, pp. 157–197. Academic Press, New York (1968).
11. N. A. Gorelova and J. Bures, Spiral waves of spreading depression in the isolated chicken retina, *J. Neurobiol.* **14**, 353–363 (1983).
12. A. L. Hodgkin and A. F. Huxley, A quantitative description of membrane current and its application to conduction and excitation in nerve, *J. Physiol.* **117**, 500–544 (1952).
13. W. Jahnke, W. E. Skaggs and A. T. Winfree, Chemical vortex dynamics in the Belousov–Zhabotinsky reaction and in 2- variable Oregonator model, *J. Phys. Chem.* **93**, 740–749 (1989).
14. W. Jahnke and A. T. Winfree, A survey of spiral-wave behavior in the Oregonator model, *Int. J. Bifurcation & Chaos* **1**, 445–466 (1991).
15. A. N. Kolmogorov, I. E. Petrovsky and N. S. Piskunov, Studying of diffusion equation connected with increasing of substance quantity, and its application to one biological problem, *Bull. Moscow State Univ., ser. A, Math. & Mech.* **1**, 1–25 (1937).
16. V. I. Krinsky, I. R. Efimov and J. Jalife, Vortices with linear cores in excitable media, *Proc. Roy. Soc.* **A437**, 645–655 (1992).
17. J. Lechleiter, S. Girard, E. Peralta and D. Clapham, Spiral calcium wave propagation and annihilation in Xenopus laevis oocytes, *Science* **252**, 123–126 (1991).

18. E. Lugosi, Analysis of meandering in Zykov kinetics, *Physica* **D40**, 331–337 (1989).
19. S. C. Muller and Th. Plesser, Dynamics of spiral centers in the ferroin-catalyzed Belousov–Zhabotinsky reaction, in *Nonlinear Wave Processes in Excitable Media*, edited by A. Holden, M. Markus and H. Othmer. Plenum, New York (1991).
20. A. V. Panfilov and A. V. Holden, Spatiotemporal irregularity in a two-dimensional model of cardiac tissue, *Int. J. Bifurcation & Chaos* **1**, 219–225 (1991).
21. H. H. Rotermund, W. Engel, M. Kordersch and G. Ertl, Imaging of spatio–temporal pattern evolution during carbon monoxide oxidation on platinum, *Nature, Lond.* **343**, 355–357 (1990).
22. G. N. Sharp and R. W. Joyner, Simulated propagation of cardiac action potential, *Biophys. J.* **31**, 403–424 (1980).
23. G. S. Skinner and H. L. Swinney, Periodic to quasiperiodic transition of chemical spiral rotation, *Physica* **D48**, 1 (1990).
24. M. Spach and P. C. Dolber, The relation between propagation in anisotropic cardiac muscle and the vulnerable period of reentry, in *Cardiac Electrophysiology and Arrhythmias*, edited by D. P. Zipes and J. Jalife, pp. 241–252. Grune & Stratton, New York (1985).
25. R. Suzuki, S. Sato and J. Nagumo, Electrochemical active network (in *Notes of IECE Japan Professional Group on NonLinear Theory*, 26 Feb (1963). (in Japanese)
26. B. van der Pol and J. van der Mark, The heartbeat considered as a relaxation oscillation, and an electrical model of the heart. *Phil. Mag.* (ser. 7) **6**, 763–775 (1928).
27. N. Wiener and A. Rosenblueth, The mathematical formulation of the problem of conduction of impulses in a network of connected excitable elements, specifically in cardiac muscle, *Arch. Inst. Cardiol. Mexico* **16**, 205–265 (1946).
28. A. T. Winfree, Spiral waves in chemical activity, *Science* **175**, 634 (1972).
29. A. T. Winfree, Electrical instability in cardiac muscle: Phase singularities and rotors, *J. Theor. Biol.* **138**, 353–405 (1989).
30. A. T. Winfree, Vortex action potential in normal ventricular muscle: mathematical approaches to cardiac arrhythmias, edited by J. Jalife, *Ann. NY Acad. Sci.* **591**, 190–207 (1990).
31. A. M. Zhabotinskii and A. N. Zaikin, Concentration wave propagation in a two-dimensional liquid-phase self-oscillating system, *Nature Lond.* **225**, 535–537 (1970).
32. V. S. Zykov, Cycloidal circulation of spiral waves in an excitable medium, *Biofizika* **31**, 862–865 (1986).
33. V. S. Zykov, *Simulation of Wave processes in Excitable media*, Manchester University Press, Manchester (1988).
34. V. S. Zykov and O. L. Morozova, Kinematic method for stability investigation of spiral autowaves, *Nonlinear Biol.* **1**, 1 (1990).
35. R. A. Fisher, The wave of advance of advantageous genes, *Ann. Eugenics* **7**, 355–369 (1937).
36. O. Selfridge, Studies of flutter and fibrillation, *Arch. Inst. Cardiol. Mexico* **18**, 177–187 (1948).
37. I. S. Balakhovsky, Several modes of excitation movement in the ideal excitable tissue. *Biophys.* **10**, 1175–1179 (1965).
38. V. I. Krinsky, Spread of excitation in an inhomogeneous medium, *Biofizika* **11**, 676–683 (1966).
39. A. T. Winfree, Varieties of spiral wave behavior in excitable media, *Chaos* **1**, 303–334 (1991).
40. F. B. Gul'ko and A. A. Petrov, Mechanism of formation of closed pathways of conduction in excitable media, *Biofizika* **17**, 261–270 (1972).

APPENDIX

Equations for the currents in Beeler–Reuter model

Dimensionless variables – x_1, m, h, j, d, and f describing the activation and inactivation of ionic currents are included in the equations as follows:

1. Time-activated outward current with the activation parameter – x_1:

$$i_{x_1} = x_1 0.8 \frac{e^{0.04(V+77)} - 1}{e^{0.04(V+35)}} \tag{A.1}$$

2. Initial fast inward current, carried primarily by sodium ions with the parameters of activation (m) and inactivation (h, j)

$$i_{Na} = (g_{Na} m^3 h j + g_{NaC})(V - E_{Na}) \tag{A.2}$$

where $g_{Na} = 4.0\ \mathrm{mS\,cm^{-2}}$, $g_{NaC} = 0.003\ \mathrm{mS\,cm^{-2}}$, $E_{Na} = 50\ \mathrm{mV}$.

Secondary or slow inward current, carried mainly (but not completely) by calcium ions with the parameters of activation and inactivation d and f, respectively:

$$i_S = g_S d f (V - E_S), \tag{A.3}$$

where $g_S = 0.09\ \mathrm{mS\,cm^{-2}}$, $E_S = -82.3 - 13.0287 \ln [\mathrm{Ca}]$.

The time-independent potassium-outward current is determined by the potential:

$$i_{K_1} = 0.35\left\{4\frac{e^{0.04(V+85)} - 1}{e^{0.08(V+53)} + e^{0.04(V+53)}} + 0.2\frac{V + 23}{1 - e^{-0.04(V+23)}}\right\} \tag{A.4}$$

Parameters $\bar{y}_i$ and τ_i are determined in terms of the rate constants:

$$\tau_i = \frac{1}{(\alpha_i + \beta_i)} \quad \text{and} \quad \bar{Y}_i = \frac{\alpha_i}{(\alpha_i + \beta_i)} \tag{A.5}$$

where

$$\alpha_i, \beta_i = \frac{C_1 e^{C_2(V+C_3)} + C_4(V + C_5)}{e^{C_6(V+C_3)} + C_7}, \tag{A.6}$$

The values of coefficients C_j are given in Table A1.

The model was extended to incorporate diffusion with respect to the potential with the coefficient $D = a/2RC$, where a is the cell radius (2.5–12.5 μm), R = specific axial resistivity (200 Ωcm), C = specific membrane capacitance (1 μF cm^{-2}) [22]. For calculation, we took the diffusion coefficient to be $D = 0.1$ mm^2 ms^{-1}.

In the equations, currents (i) are measured in μA cm^{-2} voltage (E, V, E_{Na}) in mV, time (t, τ_i) are in ms, rate constant (α_i, β_i) are in ms^{-1}, conductances (g_S, g_{Na}, g_{NaC}) are in mS cm^{-2}, $[Ca]_i$ is in mole^{-1}.

Table A1.

	C_1 (ms)$^{-1}$	C_2 (mV)$^{-1}$	C_3 (mV)	C_4 (mV ms)$^{-1}$	C_5 (mV)	C_6 (mV)$^{-1}$	C_7
α_{x_1}	0.0005	0.083	50	0	0	0.057	1
β_{x_1}	0.0013	−0.06	20	0	0	−0.04	1
α_m	0	0	47	−1	47	−0.1	−1
β_m	40	−0.056	72	0	0	0	0
α_h	0.126	−0.25	77	0	0	0	0
β_h	1.7	0	22.5	0	0	−0.082	1
α_j	0.055	−0.25	78	0	0	−0.2	1
β_j	0.3	0	32	0	0	−0.1	1
α_d	0.095	−0.01	−5	0	0	−0.072	1
β_d	0.07	−0.017	44	0	0	0.05	1
α_f	0.012	−0.008	28	0	0	0.15	1
β_f	0.0065	−0.02	30	0	0	−0.2	1